Monthly Notices
of the
ROYAL ASTRONOMICAL SOCIETY

MNRAS **492,** 1761–1769 (2020)
Advance Access publication 2019 December 23

doi:10.1093/mnras/stz3545

TOI-222: a single-transit *TESS* candidate revealed to be a 34-d eclipsing binary with CORALIE, EulerCam, and NGTS

Monika Lendl [1,2★] François Bouchy,[1] Samuel Gill,[3,4] Louise D. Nielsen [1] Oliver Turner,[1] Keivan Stassun [5,6] Jack S. Acton,[7] David R. Anderson [3,4] David J. Armstrong [3,4] Daniel Bayliss [3,4] Claudia Belardi,[7] Edward M. Bryant,[3,4] Matthew R. Burleigh,[7] Alexander Chaushev,[8] Sarah L. Casewell,[7] Benjamin F. Cooke,[3,4] Philipp Eigmüller,[8] Edward Gillen [9] Michael R. Goad,[7] Maximilian N. Günther,[10†] Janis Hagelberg [1] James S. Jenkins [11,12] Tom Louden [3,4] Maxime Marmier,[1] James McCormac,[3,4] Maximiliano Moyano,[13] Don Pollacco,[3,4] Liam Raynard [7] Rosanna H. Tilbrook,[7] Stéphane Udry,[1] Jose I. Vines,[11] Richard G. West [3,4] Peter J. Wheatley [3,4] George Ricker,[10] Roland Vanderspek,[10] David W. Latham,[14] Sara Seager,[10,15,16] Josh Winn,[17] Jon M. Jenkins,[18] Brett Addison,[19] César Briceño,[20] Rafael Brahm,[21,22] Douglas A. Caldwell,[18,23] John Doty,[24] Néstor Espinoza,[25,26] Bob Goeke,[10] Thomas Henning,[26] Andrés Jordán,[22,27] Akshata Krishnamurthy,[10] Nicholas Law,[28] Robert Morris,[18,23] Jack Okumura,[19] Andrew W. Mann,[28] Joseph E. Rodriguez,[14] Paula Sarkis,[26] Joshua Schlieder,[29] Joseph D. Twicken,[18,23] Steven Villanueva, Jr.,[10‡] Robert A. Wittenmyer,[19] Duncan J. Wright[19] and Carl Ziegler[30]

Affiliations are listed at the end of the paper

Accepted 2019 December 13. Received 2019 December 13; in original form 2019 October 11

ABSTRACT

We report the period, eccentricity, and mass determination for the *Transiting Exoplanet Survey Satellite (TESS)* single-transit event candidate TOI-222, which displayed a single 3000 ppm transit in the *TESS* 2-min cadence data from Sector 2. We determine the orbital period via radial velocity measurements (P = 33.9 d), which allowed for ground-based photometric detection of two subsequent transits. Our data show that the companion to TOI-222 is a low-mass star, with a radius of $0.18^{+0.39}_{-0.10}$ $R_\odot$ and a mass of 0.23 ± 0.01 $M_\odot$. This discovery showcases the ability to efficiently discover long-period systems from *TESS* single-transit events using a combination of radial velocity monitoring coupled with high-precision ground-based photometry.

Key words: techniques: photometric – stars: individual: TOI-222 – planetary systems.

1 INTRODUCTION

Even though the probability of an exoplanet to transit across its host plummets for long orbital periods, space-based transit surveys such as *COROT* (Baglin et al. 2006) and Kepler (Borucki et al. 2010) have succeeded in detecting a number of long-period transiting planets as they monitor large fields continuously for extended periods of time. Unlike its predecessors, the Transiting Exoplanet Survey Satellite (*TESS*; Ricker et al. 2014) is optimized for bright stars. From its recently completed survey of the Southern ecliptic hemisphere, over 1000 promising exoplanet candidates, including multiplanet candidate systems, have been reported as *TESS* objects of interest (TOIs). A number of the candidates have now also been confirmed as bona fide transiting planets via radial velocity (RV) measurements, for example, pi Mensae c (Gandolfi et al. 2018; Huang et al. 2018), HD 202772A b (Wang et al. 2019), and HD 1397 b (Brahm et al. 2019; Nielsen et al. 2019).

★ E-mail: monika.lendl@unige.ch
† Juan Carlos Torres Fellow.
‡ Pappalardo Fellow.

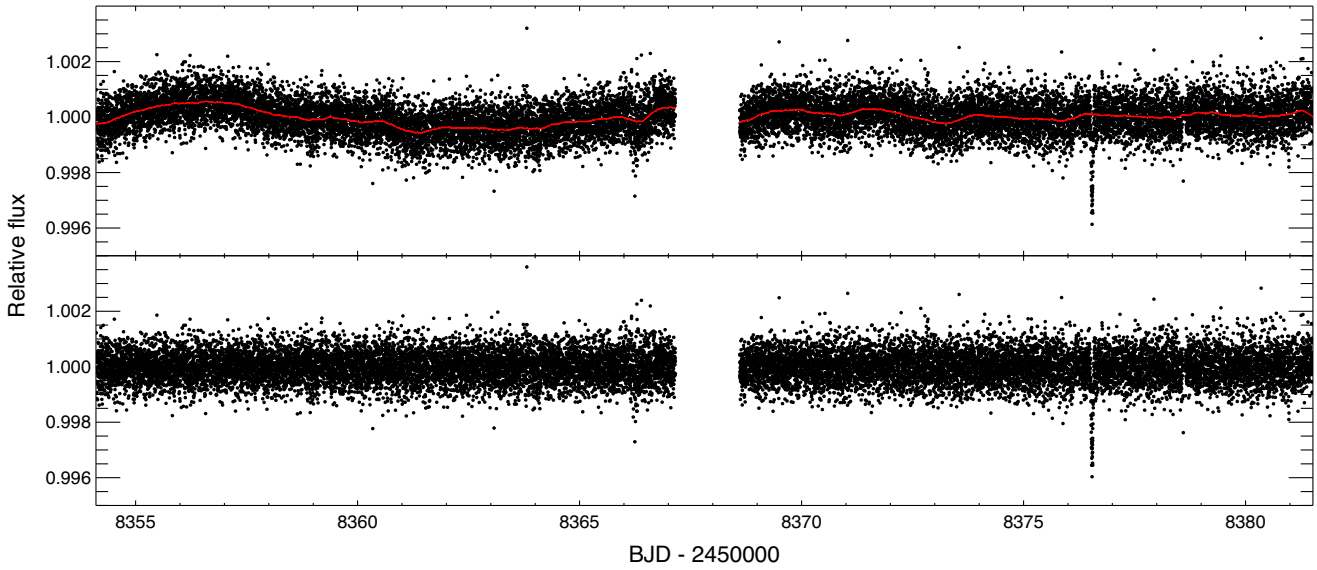

Figure 1. *TESS* data of TOI-222. The top panel shows the uncorrected data in black with the 10-h boxcar applied to correct for stellar and instrumental systematics in red. The bottom panel shows the corrected *TESS* data.

As predicted by simulations (Cooke et al. 2018; Villanueva, Dragomir & Gaudi 2019), *TESS* also detected a number of promising exoplanet candidates for which only a single-transit event was observed. These 'Monotransits' do not provide well-determined periods, although period estimates can be derived using knowledge of the host star and transit parameters (Osborn et al. 2016). Since the time coverage of *TESS* is limited to 27 d for large parts of the sky, these single-transit event candidates provide longer period planetary systems and eclipsing binaries. The confirmation of monotransit candidates through the observation of a second transit is challenging as the planetary period is only loosely constrained. This task can be made easier by monitoring the primary's RV in order to constrain the spectroscopic orbit and predict the times of subsequent transit events.

In this work, we present the mass and period determination of TOI-222: a TOI identified as a *TESS* single-transit event in Sector 2. Using spectroscopic follow-up, we determined the orbit of this low-mass eclipsing binary, leading to the recovery of the transit from subsequent photometric observations. We describe the observations and the analysis of our data in Sections 2 and 3, and place this detection into context in Section 4.

2 OBSERVATIONS

2.1 *TESS* Discovery Photometry

The V = 9.3 star HD 224286 (TIC 144440290) was observed by *TESS* in Sector 2 throughout 27.4 d. The observations have a continuous 2-min cadence, with only a short gap occurring at the centre of the sequence when observations were interrupted to allow for the data to be downlinked to the Earth. A single, approximately 3.5 mmag deep, transit event was identified and denominated TOI-222 by the *TESS* team. The transit occurred approximately 22 d after the start of the sequence, thus constraining the period of a potential planet or binary companion to be above 22 d. The long period but comparatively short total transit duration of 1.8 h, paired with a clear V shape, indicated a grazing configuration, with a larger planet or an eclipsing binary only partially transiting the star.

We used the *TESS* Science Processing Operations Center (Jenkins et al. 2016) 2-min cadence PDC light curve (Smith et al. 2012; Stumpe et al. 2014) for the subsequent analysis, and additionally filtered the time-series by a 12-h boxcar to remove a low-amplitude variation likely caused by stellar active regions rotating in and out of view. Data points obtained in transit were excluded at this step in order to avoid altering the transit shape when correcting these long-term trends. The *TESS* data are shown in Fig. 1.

2.2 High-resolution spectroscopy with CORALIE

TOI-222 was observed with the CORALIE spectrograph on the Swiss 1.2 m Euler telescope at La Silla Observatory, Chile (Queloz et al. 2001) between 2019 January 2 and June 30. CORALIE has a resolving power of $R \sim 60\,000$ and is fed by two fibres; one 2 arcsec on-sky science fibre encompassing the star and another that can either be connected to a Fabry–Pérot etalon for simultaneous wavelength calibration or on-sky for background subtraction of the sky flux. RVs were computed for each epoch by cross-correlating with a binary G2 mask (Pepe et al. 2002). Bisector-span, full width at half-maximum (FWHM) and other line-profile diagnostics were computed as well using the standard CORALIE pipeline. As initial observations showed a large 10 km s^{-1} RV shift over 9 d, we reduced the exposure time from 1800 to 900–300 s depending on seeing and airmass to save telescope time. We obtain a final precision of 6–20 m s^{-1}. The resulting velocities are given in Table 1 and are shown in Fig. 2. The CORALIE spectra were shifted to the stellar rest frame and stacked while weighting the contribution from each spectrum with its mean flux to produce a high-signal-to-noise spectrum for spectral characterization.

We detected significant RV variations in the CORALIE data, indicative of a low-mass stellar component orbiting the main target with a period of 33.9 d, which prompted us to proceed with photometric follow-up.

2.3 Transit recovery with EulerCam

With the system period established, we scheduled photometric observations with EulerCam, also installed at the 1.2 m Euler

Table 1. Radial velocities for TOI-222.

BJD (−2400 000)	RV (km s^{-1})	RV err (km s^{-1})	FWHM (km s^{-1})	BIS (km s^{-1})	Instrument
58486.571350	1.946 99	0.015 89	8.191 62	− 0.039 97	CORALIE
58490.540095	5.548 85	0.006 45	8.253 66	− 0.057 06	CORALIE
58495.549674	12.010 76	0.006 47	8.260 60	− 0.05091	CORALIE
58510.528803	22.298 37	0.014 79	8.231 69	− 0.00504	CORALIE
58514.527724	5.945 52	0.012 39	8.262 12	− 0.04074	CORALIE
58517.523825	1.487 04	0.012 97	8.279 96	− 0.059 66	CORALIE
58526.513423	7.986 38	0.032 71	8.314 53	− 0.093 61	CORALIE
58636.901387	20.937 34	0.018 24	8.243 19	− 0.091 94	CORALIE
58638.938599	24.242 32	0.013 93	8.239 49	− 0.008 28	CORALIE
58640.945601	27.105 96	0.018 44	8.276 72	0.004 45	CORALIE
58641.935281	28.068 41	0.015 44	8.245 95	− 0.062 31	CORALIE
58656.822502	2.422 60	0.013 50	8.318 97	− 0.028 12	CORALIE
58664.859362	11.6754	0.021 99	8.235 40	− 0.006 85	CORALIE

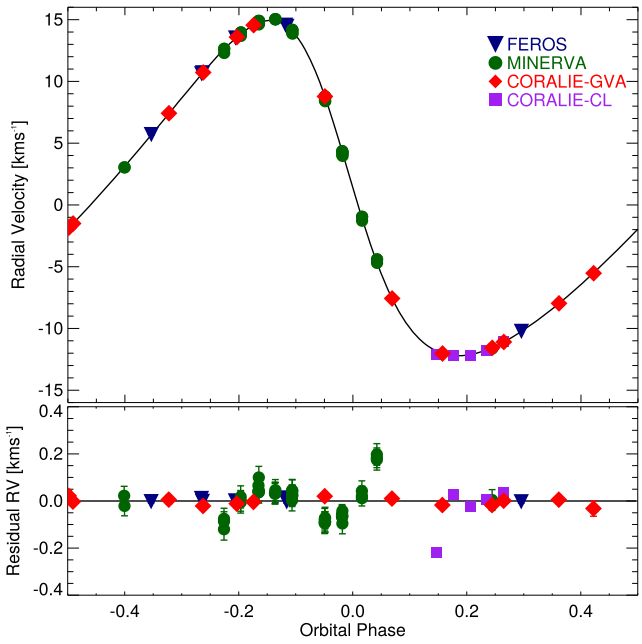

Figure 2. Radial velocities of TOI-222 together with the best-fitting RV solution (top panel), and best-fitting residuals (bottom panel). CORALIE data from the Geneva ('CORALIE-GVA') and the MPIA-Chile ('CORALIE-CL') teams were reduced with different pipelines and are shown as the red diamonds and the purple squares, respectively; FEROS data are shown as the blue triangles, and MINERVA data are shown in green. The error bars are smaller than the size of the data points in most cases.

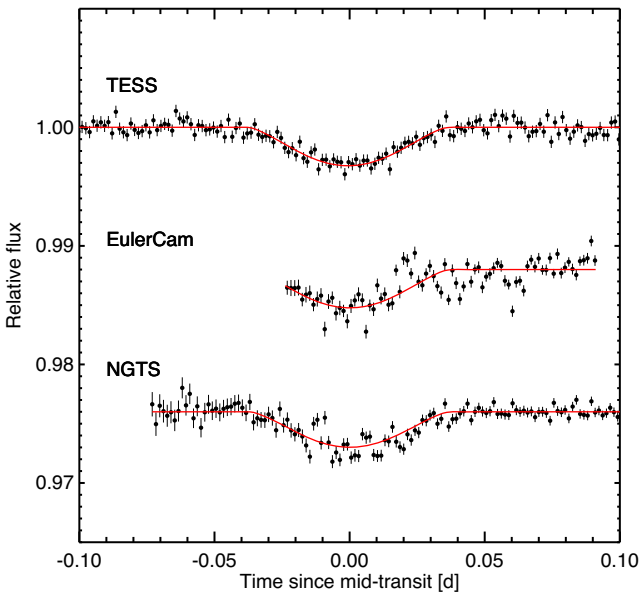

Figure 3. Photometric data used to perform a global fit of the system. These are (from top to bottom) *TESS*, EulerCam, and NGTS. All light curves have been detrended and binned into 2-min intervals.

telescope, with the goal of detecting a second transit of the low-mass companion in front of its host. The observations were carried out throughout 2.8 h on 2019 June 13, covering approximately 75 per cent of the predicted 1σ transit window. We used an Cousins I filter, 20 s exposures and applied a large defocus to avoid saturating the target while keeping a reasonable observation efficiency. For details on the instrument and the data analysis routines used to extract relative aperture photometry, please refer to Lendl et al. (2012). We detected a flux drop of ∼3.5 mmag during first half of the sequence, having a depth compatible with that of the *TESS* measurement. The egress occurred approx. 42 min (or 3.8σ) earlier than predicted, indicating a slightly shorter planetary period. The EulerCam light curve is shown in Fig. 3, and the data set is presented in Table 2.

2.4 Transit confirmation with NGTS

TOI-222 was initially scheduled for a blind search with NGTS to recover the orbital period following its designations as a single-transit object of interest from *TESS*. We obtained 37 nights of single-telescope observations (18 510 images with 10-s exposures).

Once the system's period was known, we scheduled NGTS observations to cover the next primary eclipse of TOI-222, occurring on 2019 July 17. In total, 10 telescopes were used to simultaneously observe the primary eclipse, collecting over 10 000 individual data points with an exposure time of 10 s each. The data were reduced using the CASUTOOLS[1] photometry package and we applied the SYSREM algorithm (Tamuz, Mazeh & Zucker 2005) to detrend the data. For more details on NGTS, please refer to Wheatley et al. (2018). The resulting light curve was binned to 2 min and detrended using a third-order time polynomial, obtaining an RMS of ∼450 ppm.

[1] http://casu.ast.cam.ac.uk/surveys-projects/software-release

Table 2. EulerCam photometry. The full table is available from the online version of this paper.

BJD (−245000)	Flux	Flux error	*x*-shift (pixel)	*y*-shift (pixel)	airmass	FWHM (pixel)	sky flux (e^-)	exposure time (s)
8647.819731	0.9964 30	0.0011 89	− 0.76	2.31	1.41	14.09	42.96	20.00
8647.820159	0.9935 07	0.0011 86	− 0.45	3.02	1.41	15.29	42.88	20.00
8647.820589	0.9980 77	0.0011 91	− 1.33	1.81	1.41	14.37	42.58	20.00
8647.821005	0.9950 25	0.0011 75	0.24	0.92	1.40	15.59	42.72	20.00
8647.821431	0.9948 32	0.0011 74	3.46	− 1.46	1.40	15.77	41.77	20.00

Table 3. NGTS photometry, binned into 2-min intervals. The full table is available from the online version of this paper.

BJD	Flux	Flux error
2458681.682801	1.0006 19	0.0010 27
2458681.684190	0.9989 42	0.0009 92
2458681.685579	1.0004 91	0.0009 73
2458681.686967	1.0000 34	0.0009 56
2458681.688356	0.9996 49	0.0009 28

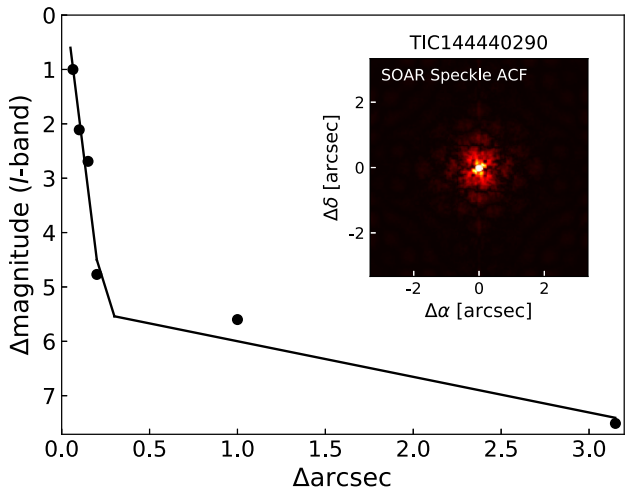

Figure 4. The 5σ detection sensitivity to companion stars to TOI-222 for the SOAR speckle observation. Inset is the speckle autocorrelation function derived from the SOAR observation. No stars were detected within 3 arcsec of TOI-222.

We clearly detect the primary eclipse of TOI-222 with NGTS, confirming the slightly shorter period and distinct V-shape of the eclipse. The NGTS data are shown in Fig. 3 and the data are given in Table 3.

2.5 Additional high-resolution spectroscopy

2.5.1 High-resolution spectroscopy with FEROS and CORALIE

The RV variation of TOI-222 was also monitored using the FEROS spectrograph (R = 48 000; Kaufer et al. 1999) mounted on the MPG 2.2 m telescope installed in La Silla Observatory. A total number of seven spectra were obtained between 2019 June 4 and July 13. The adopted exposure time was of 300 s that produced spectra with a typical SNR per resolution element of 130. Observations were performed using the simultaneous calibration mode in which a comparison fiber is illuminated with a Thorium–Argon lamp in order to trace the instrumental variations during the science exposure. Next to these data, we also obtained an additional four data points with CORALIE under Chilean time. These data were processed with the automated CERES package (Brahm, Jordán & Espinoza 2017) that performs the optimal extraction, wavelength calibration, and computation of precision radial velocities using the cross-correlation technique.

2.5.2 High-resolution spectroscopy with MINERVA–Australis

A total of 60 spectra of TOI-222 were obtained at 15 epochs between 2019 May 11 and July 18, using the MINERVA–Australis telescope array at Mt. Kent Observatory in Queensland, Australia (Wittenmyer et al. 2018; Addison et al. 2019). All of the telescopes in the MINERVA–Australis array simultaneously feed a single Kiwispec R4-100 high-resolution (R 80 000) spectrograph with wavelength coverage from 500 to 630 nm over 26 echelle orders. Light from each of the four telescopes is delivered to individual fibres (numbered 3, 4, 5, and 6), and calibration is achieved via a simultaneous Thorium–Argon lamp illuminating fibres 1 and 7. We derived radial velocities for each telescope using the least-squares analysis of Anglada-Escudé & Butler (2012) and corrected for spectrograph drifts with simultaneous Thorium–Argon arc lamp observations. TOI-222 was observed simultaneously with up to four telescopes, with one or two 30-min exposures per epoch. The radial velocities from each telescope are given in Table 1 labelled by their fibre number. Each telescope (fibre) has its own velocity zero-point that is modelled as a free parameter, and the mean uncertainty of the 60 MINERVA–Australis observations is 4.5 m s^{-1}. Additional scatter in the MINERVA data was introduced by a power cut at the observatory.

2.6 Speckle imaging

Nearby stars that fall within the same 21 arcsec *TESS* pixel as TOI-222 could contaminate the *TESS* photometry, resulting in a reduced transit depth. We searched for unaccounted companions to TOI-222 with SOAR speckle imaging (Tokovinin 2018) on 2019 May 18 UT, observing in a similar visible bandpass as *TESS*. Additional details of the observation are available in Ziegler et al. (2019). We detected no nearby stars within 3 arcsec of TOI-222. The 5σ detection sensitivity and the speckle autocorrelation function from the SOAR observation are plotted in Fig. 4.

3 SYSTEM ANALYSIS

3.1 Properties of the primary

We used the CORALIE spectra to derive atmospheric parameters for the primary. Each spectrum was corrected into the laboratory

Table 4. Stellar properties of the primary.

Property	Value	Source
Astrometric properties		
RA	$23^h56^m38\overset{s}{.}99$	2 MASS
Dec.	$-44°43'09\overset{''}{.}81$	2MASS
2MASS I.D.	J23563876-4443086	2MASS
μ_{RA} (mas yr^{-1})	161.769 ± 0.049	UCAC4
$\mu_{Dec.}$ (mas yr^{-1})	$-75.541.0 \pm 0.055$	UCAC4
Photometric properties		
V (mag)	9.528 ± 0.37	APASS
B (mag)	10.009 ± 0.013	APASS
g (mag)	9.609 ± 0.03	APASS
r (mag)	9.424 ± 0.392	APASS
i (mag)	9.333 ± 0.412	APASS
G (mag)	9.15167 ± 0.00035	*Gaia*
T (mag)	8.723 ± 0.017	*TESS*
J (mag)	8.144 ± 0.019	2MASS
H (mag)	7.869 ± 0.024	2MASS
K (mag)	7.7729 ± 0.021	2MASS
W1 (mag)	7.681 ± 0.029	WISE
W2 (mag)	7.763 ± 0.019	WISE
Derived properties		
T_{eff} (K)	5815 ± 85	CORALIE Spectra
[M/H]	0.11 ± 0.06	CORALIE Spectra
v sin i (km s^{-1})	3.60 ± 1.35	CORALIE Spectra
γ_{RV} (km s^{-1})	13.51423 ± 0.005	CORALIE Spectra
log g	4.5 ± 0.13	CORALIE Spectra
R_1 ($M_\odot$)	1.047 ± 0.031	SED fit
M_1 ($R_\odot$)	1.07 ± 0.08	TO
ρ_1 ($\rho_\odot$)	0.94 ± 0.17	
Distance (pc)	$84^{+0.3}_{-0.3}$	BJ

*Notes.*2MASS (Skrutskie et al. 2006); UCAC4 (Zacharias et al. 2013); APASS (Henden & Munari 2014); WISE (Wright et al. 2010); *Gaia* (Gaia Collaboration 2016).
ER = empirical relations using Benedict et al. (2016) and Mann et al. (2015).
TO = interpolated from Torres et al. (2010).
BJ = from Bailer-Jones et al. (2018).

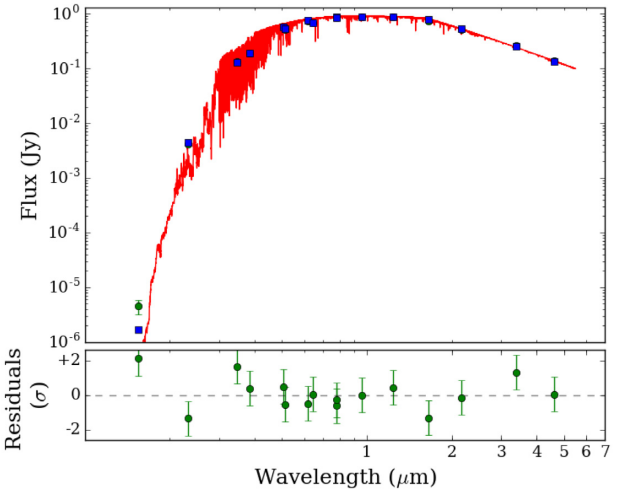

Figure 5. The fitted spectral energy distribution (the red line) for TOI-222 based on the photometric data (the green points) presented in Table 4. The blue squares show the model flux at the wavelengths of the photometric data.

reference frame and co-added on to a common wavelength range. Maximum and median filters were applied to identify continuum regions that were fitted with spline functions (one every nm) to normalize the spectra (a standard function within ispec v20161118; Blanco-Cuaresma et al. 2014). We used wavelet analysis (Gill, Maxted & Smalley 2018) to determine the best-fitting atmospheric parameters for the host star, which works by comparing the wavelet coefficients of the target spectrum to a grid of model spectra. We re-sample between 450 and 650 nm with 2^{17} values and co-add the spectra. We calculate the wavelet coefficients Wi = 4–14 and fit the same coefficients with model spectra (identical to those used in Gill et al. 2018, 2019) in a Bayesian framework. We initiated 100 walkers and generated 10 000 draws as a burn-in phase. We generated a further 10 000 draws to sample the posterior probability distribution (PPD) for the stellar effective temperature (T_{eff}), metallicity ([Fe/H]), projected rotational velocity (V sin i), and surface gravity (log g). Gill et al. (2018) note an [Fe/H] offset of −0.18 dex, which we correct for by adding 0.18 dex to the PPD for [Fe/H]. The wavelet method for CORALIE spectra can determine T_{eff} to a precision of 85 K, [Fe/H] to a precision of 0.06 dex and V sin i to a precision of 1.35 km s^{-1} for stars with V sin $i \geq 5$ km s^{-1}. However, measurements of log g from wavelet analysis are not reliable beyond confirming dwarf-like gravity (log g ≈ 4.5 dex). Subsequently, we fit the wings of the magnesium triplets with spectral synthesis by fixing T_{eff}, [Fe/H] and V sin i and changing log g until an acceptable fit was found. The inferred values are listed in Table 4.

For an empirical determination of the stellar radius, we performed an analysis of the broad-band spectral energy distribution (SED) together with the *Gaia* parallax, following the procedures described in Stassun & Torres (2016), Stassun, Collins & Gaudi (2017), and Stassun et al. (2018). We pulled the B_TV_T magnitudes from *Tycho-2*, the *BVgri* magnitudes from APASS, the JHK_S magnitudes from *2MASS*, the W1–W4 magnitudes from *WISE*, the G magnitude from *Gaia*, and the FUV and NUV fluxes from *GALEX*. Together, the available photometry spans the full stellar SED over the wavelength range 0.15–22 μm. We performed a fit using Kurucz stellar atmosphere models, with the priors on T_{eff}, log g, and [Fe/H] from the spectroscopic analysis. The remaining free parameter is the extinction (A_V), which we limited to the maximum line-of-sight extinction from the Schlegel, Finkbeiner & Davis (1998) dust maps. The resulting fit is good with a reduced χ^2 of 3.9, and a best-fitting extinction of $A_V = 0.02 \pm 0.02$. Integrating the (unextincted) model SED gives the bolometric flux at Earth of $F_{bol} = 5.15 \pm 0.12 \times 10^{-9}$ erg s^{-1} cm^{-2}. Taking the F_{bol} and T_{eff} together with the *Gaia* parallax, adjusted by +0.08 mas to account for the systematic offset reported by Stassun & Torres (2018), gives the stellar radius as $R = 1.047 \pm 0.031$ $R_\odot$.

We verified the above SED fitting of TOI-222 with the method outlined in Gillen et al. (2017), using the PHOENIX v2 set of models with the information available from blended catalogue photometry and *Gaia* photometric and astrometric data listed in Table 4 (see Fig. 5). Both methods are in very good agreement.

In addition, we can estimate the stellar mass from the eclipsing-binary-based empirical relations of Torres, Andersen & Giménez (2010), which gives $M = 1.07 \pm 0.08$ $M_\odot$, This, together with the empirical radius above, gives the mean stellar density $\rho = 0.94 \pm 0.10\rho_\odot = 1.32 \pm 0.14$ gcm^{-3}.

3.2 Orbital solution

3.2.1 MCMC framework

We used the **CO***de for transiting exopla***N***et* **AN***alysis*, a Markov Chain Monte Carlo (MCMC) framework to carry out a simultaneous analysis of transit and RV data. *CONAN* is based on the transit analysis code described in Lendl et al. (2017), with the added capacities of jointly analysing RV and transit data and thus deriving consistent system properties. *CONAN* is capable of simultaneously modelling multiple transit and RV data sets, deriving global system properties while allowing for independent baseline models for each data set. The MCMC engine can be set to either *emcee* (Foreman-Mackey et al. 2017) or *MC3* (Cubillos et al. 2017).

To compute transit and RV models, *CONAN* uses the routines of Kreidberg (2015) and a Keplerian, respectively. The MCMC jump (i.e. fitted) parameters are

(i) the stellar-to-planetary radius ratio, R_p/R_*,
(ii) the timing of mid-transit, T_0,
(iii) the orbital inclination, *inc*,
(iv) the normalized orbital semimajor axis, a/R_*,
(v) the planetary orbital period, *P,*
(vi) the RV amplitude, *K,*
(vii) $\sqrt{e}\sin\omega$ and $\sqrt{e}\cos\omega$ to derive the eccentricity e and the argument of periastron ω,
(viii) the combination of the systemic RV, γ, together with the RV zero-point $RV_{0,i}$ of each RV data set, $\gamma + RV_{0,i}$, and
(ix) the linear combinations $c_1 = 2u_1 + u2$ and $c_2 = u_1 - u_2$ of the quadratic limb-darkening coefficients u_1 and u_2 (Holman et al. 2006).

Most photometric time-series are affected by some degree of correlated noise, of observational (e.g. differential effects due to reference stars differing in colour), instrumental (e.g. telescope pointing jitter paired with flat-field inhomogeneities) or stellar (e.g. rotational variability) origin. We account for these effects using parametric baseline models in the form of a combination polynomials or trigonometric functions in one or several state variables (e.g. time, stellar FWHM, coordinate shifts, airmass, see e.g. Gillon et al. 2010; Lendl et al. 2017). The coefficients can either be found via least-squares minimization at each MCMC step, or included as MCMC jump parameters. While both approaches fulfil the requirement that baseline coefficients are fit at the same time as the transit parameters (and therefore assure that uncertainties in the baseline parameters are propagated to the inferred transit parameters), the earlier leads to enhanced convergence while being computationally more expensive, the latter allows to trace correlation between the baseline model and transit parameters. Convergence of the MCMC chains is checked with the Gelman & Rubin test (Gelman & Rubin 1992).

We also include two approaches to compensate for excess noise. Either, the user can choose to scale the errors via the β_r, β_w method that consists in comparing the binned and non-binned light curve residuals (Winn et al. 2008; Gillon et al. 2010), or decide to quadratically add extra noise to each light curve to reach a reduced chi-square equal to unity. Both approaches assure correct weighing between individual data sets. The latter does so on the basis of assuming white Gaussian noise, while the former compensates for excess red noise and often results in χ_{red} values below unity. Also, RV measurements are often affected by excess noise, most prominently due to stellar activity. CONAN allows to account for this *RV jitter* by adding excess noise quadratically to the RV errors such that $\chi^2_{red,RV} = 1$ is reached.

To compute physical properties from the fitted data, CONAN uses input values for M_* and R_*, and draws from Gaussian distributions centred on these values, and with a user-specified width, for each parameter state output by the MCMC. Here, one may define both M_* and R_*, or define one and fit for the other using the information contained in the transit light curve.

3.3 The TOI-222 system

We used *CONAN* together with the stellar parameters inferred from the CORALIE data as described in Section 3.1 to derive the properties of the TOI-222 system. Stellar limb darkening was treated using a quadratic law, with the coefficients derived using the procedures by Espinoza & Jordán (2015), and held fixed during the analysis. RV data from CORALIE and FEROS were fitted without the need of including a trend, however, the MINERVA RVs were affected by an instrumental drift that we compensated by fitting (individually) quadratic drifts to the RV values of fibres 3, 4, and 6 and a linear drift to RVs from fibre 5. The photometric baseline models used were a third-order time polynomial for the NGTS data, and a combination of second-order polynomials in the stellar FWHM and the sky flux for the EulerCam data. The previously detrended *TESS* data were cut to a shorter sequence of 1-d length centred on the transit and only a constant flux offset was fitted. The light curves are shown in Fig. 3. To aid convergence, we first carried out a least-squares minimization and used the resulting values as starting points for the MCMC chains.

The primary eclipse of TOI-222 is highly grazing, with an impact parameter larger than unity. This inhibits the precise measurement of the secondary star's radius as the radius ratio is strongly correlated with the system's inclination (a larger secondary will create a similarly shallow eclipse when the impact parameter of the eclipse is larger). This means that, albeit the exquisite precision of the photometry, the secondary radius is only loosely constrained. The parameters of the TOI-222 system are summarized in Table 5.

4 CONCLUSIONS AND OUTLOOK

We present the ephemeris recovery and orbital characterization of the single-transit *TESS* candidate TOI-222 by means of RV monitoring with CORALIE and ground-based photometry with EulerCam and NGTS. TOI-222 is a binary system with a low-mass eclipsing component orbiting a V = 9.3 G2V star in a 33.9-d orbit, showing ∼3500 ppm-deep grazing eclipses. By observing simultaneously with 10 individual 20 cm NGTS telescopes, we obtain a photometric precision better than 500 ppm per 2-min bin. This demonstrates that we can reach the precision needed to retrieve small-amplitude signals using this technique. While TOI-222 counts as a false-positive in the realm of exoplanet discoveries, this detection highlights that long-period single-transit events can be efficiently recovered from the ground, provided well-coordinated high-precision RV and photometric facilities are available. In the light of the several hundreds of predicted single-transit candidates from *TESS* (Cooke et al. 2018; Villanueva et al. 2019), this opens up a promising avenue for the confirmation of long-period transiting planets.

TOI-222, and future similar discoveries, are particularly exciting as they represent some of the most isolated M-dwarfs with physical properties measured using radial velocities and eclipse photometry. Non-transiting low-mass binaries characterized with RV measurements and/or astrometry require mass–radius–luminosity relations

Table 5. Properties of the TOI-222 system from a global MCMC analysis.

Jump parameters	
T_0, (BJD – 2450000)	$8376.5444^{+0.0005}_{-0.0006}$
Radius ratio, R_1/R_2	$0.17^{+0.37}_{-0.10}$
Inclination (deg)	$88.1^{+0.14}_{-0.84}$
a/R_1	$42.7^{+2.5}_{-1.8}$
Period (d)	$33.91237^{+0.00008}_{-0.00013}$
$\sqrt{e}\sin\omega$	$0.5018^{+0.0001}_{-0.0004}$
$\sqrt{e}\cos\omega$	$0.1871^{+0.0004}_{-0.0002}$
RV amplitude K (km s^{-1})	13.574 ± 0.003
Primary parameters from spectral analysis	
R_1 ($R_\odot$)	1.047 ± 0.031
M_1 ($M_\odot$)	1.07 ± 0.08
Derived parameters	
R_2 ($R_\odot$)	$0.18^{+0.39}_{-0.10}$
M_2 ($M_\odot$)	0.23 ± 0.01
Orbital semimajor axis (au)	$0.208^{+0.014}_{-0.010}$
Primary eclipse impact parameter	$1.03^{+0.37}_{-0.11}$
Orbital eccentricity	$0.2868^{+0.00008}_{-0.00027}$
Argument of periastron (deg)	$69.55^{+0.02}_{-0.05}$
Fixed quadratic limb-darkening parameters	
$u_{1,\,TESS}$	0.3618
$u_{2,\,TESS}$	0.2180
$u_{1,\,IC}$	0.3679
$u_{2,\,IC}$	0.2175
$u_{1,\,NGTS}$	0.4561
$u_{2,\,NGTS}$	0.2067
Radial velocity zero-point offsets[a], (m s^{-1})	
CORALIE (CERES)	-11 ± 476
FEROS	13 ± 332
MINERVA3	5817 ± 300
MINERVA4	5822 ± 300
MINERVA5	329 ± 349
MINERVA6	6153 ± 293

[a]Relative to CORALIE.

(e.g. Delfosse et al. 2000 or Southworth 2009) that carry relatively large uncertainties and can often be unreliable. Some M-dwarfs around F-/G-type stars have been measured to be hotter and larger than predicted by stellar evolution models. Of those measured within the EBLM project (Hebb et al. 2012), two stars (WASP−30B and J1013 + 01) appear to be inflated, and a third (J0113 + 31) is measured to be $\sim 600\,K$ hotter than expected. A similar result was also seen for KIC1571511 (Ofir et al. 2012) using high-precision optical photometry from the Kepler space telescope. The favoured explanation lies with magnetic activity, as M-dwarfs in binary systems can be kept in fast rotation regime, by tidal-induced spin-orbit synchronization, generating an enhanced magnetic field via dynamo action (Chabrier, Gallardo & Baraffe 2007). The effect of this is two-fold: an inhibition of convection in the (almost) fully convective core and higher spot coverage (Gough & Tayler 1966). Compared to these objects, TOI-222 has a relatively large orbital period and thus a large orbital separation. TOI-222 is also not in synchronous rotation, as the spectroscopically determined $V \sin i$ implies faster rotation, with a period of at least ∼14.7 d. Due to the grazing configuration, the TOI-222 system itself is not suited to probe trends between radius inflation and orbital separation. Similar systems, however, that are likely to be found from *TESS* single-transit events in the future, will be instrumental in building a larger sample of well-detatched low-mass eclipsing binaries needed to carry out these studies.

ACKNOWLEDGEMENTS

We thank the Swiss National Science Foundation (SNSF) and the Geneva University for their continuous support to our planet search programs. Contributions at the University of Geneva by FB, LN, ML, OT, and SU were carried out within the framework of the National Centre for Competence in Research 'PlanetS' supported by the SNSF. Based on data collected under the NGTS project at the ESO La Silla Paranal Observatory. The NGTS facility is operated by the consortium institutes with support from the UK Science and Technology Facilities Council (STFC) under projects ST/M001962/1 and ST/S002642/1. The contributions at the University of Warwick by PJW, RGW, DLP, DJA, and TL have been supported by STFC through consolidated grants ST/L000733/1 and ST/P000495/1. DJA acknowledges support from the STFC via an Ernest Rutherford Fellowship (ST/R00384X/1). The contributions at the University of Leicester by MGW and MRB have been supported by STFC through consolidated grant ST/N000757/1. CAW acknowledges support from the STFC grant ST/P000312/1. TL was also supported by STFC studentship 1226157. MNG acknowledges support from MIT's Kavli Institute as a Torres postdoctoral fellow. ML acknowledges support from the Austrian Research Promotion Agency (FFG) under project 859724 'GRAPPA'. JSJ acknowledges support by Fondecyt grant 1161218 and partial support by CATA-Basal (PB06, CONICYT). JIV acknowledges support of CONICYT-PFCHA/Doctorado Nacional-21191829, Chile. RB acknowledges support from FONDECYT Post-doctoral Fellowship Project 3180246, and from the Millennium Institute of Astrophysics (MAS). AJ acknowledges support from FONDECYT project 1171208, and by the Ministry for the Economy, Development, and Tourism's Programa Iniciativa Científica Milenio through grant IC 120009, awarded to the MAS. This project has received funding from the European Research Council (ERC) under the European Union's Horizon 2020 research and innovation programme (grant 681601). The research leading to these results has received funding from the ERC under the European Union's Seventh Framework Programme (FP/2007-2013)/ERC grant 320964 (WDTracer). MINERVA–Australis is supported by Australian Research Council LIEF grant LE160100001, Discovery grant DP180100972,Mount Cuba Astronomical Foundation, and institutional partners University of Southern Queensland, UNSW Australia, MIT, Nanjing University, George Mason University, University of Louisville, University of California Riverside, University of Florida, and The University of Texas at Austin. We respectfully acknowledge the traditional custodians of all lands throughout Australia, and recognize their continued cultural and spiritual connection to the land, waterways, cosmos, and community. We pay our deepest respects to all Elders, ancestors, and descendants of the Giabal, Jarowair, and Kambuwal nations, upon whose lands the Minerva–Australis facility at Mt Kent is situated. Funding for the *TESS* mission is provided by NASA's Science Mission directorate. We acknowledge the use of public *TESS* Alert data from pipelines at the *TESS* Science Office and at the *TESS* Science Processing Operations Center. Resources supporting this work were provided by the NASA High-End Computing Program through the NASA Advanced Supercomputing Division at Ames Research Center for the production of the SPOC data products.

REFERENCES

Addison B. et al., 2019, PASP, 131, 115003
Anglada-Escudé G., Butler R. P., 2012, ApJS, 200, 15

Baglin A. et al., 2006, in 36th COSPAR Scientific Assembly, Beijing, China, p. 3749
Bailer-Jones C. A. L., Rybizki J., Fouesneau M., Mantelet G., Andrae R., 2018, AJ, 156, 58
Benedict G. F. et al., 2016, AJ, 152, 141
Blanco-Cuaresma S., Soubiran C., Heiter U., Jofré P., 2014, A&A, 569, A111
Borucki W. J. et al., 2010, Science, 327, 977
Brahm R., Jordán A., Espinoza N., 2017, PASP, 129, 034002
Brahm R. et al., 2019, AJ, 158, 45
Chabrier G., Gallardo J., Baraffe I., 2007, A&A, 472, L17
Cooke B. F., Pollacco D., West R., McCormac J., Wheatley P. J., 2018, A&A, 619, A175
Cubillos P., Harrington J., Loredo T. J., Lust N. B., Blecic J., Stemm M., 2017, AJ, 153, 3
Delfosse X., Forveille T., Ségransan D., Beuzit J.-L., Udry S., Perrier C., Mayor M., 2000, A&A, 364, 217
Espinoza N., Jordán A., 2015, MNRAS, 450, 1879
Foreman-Mackey D., Agol E., Ambikasaran S., Angus R., 2017, AJ, 154, 220
Gaia Collaboration, 2016, A&A, 595, A2
Gandolfi D. et al., 2018, A&A, 619, L10
Gelman A., Rubin D., 1992, Stat. Sci., 7, 457
Gill S., Maxted P. F. L., Smalley B., 2018, A&A, 612, A111
Gill S. et al., 2019, A&A, 626, A119
Gillen E., Hillenbrand L. A., David T. J., Aigrain S., Rebull L., Stauffer J., Cody A. M., Queloz D., 2017, ApJ, 849, 11
Gillon M. et al., 2010, A&A, 511, A3
Gough D. O., Tayler R. J., 1966, MNRAS, 133, 85
Hebb L., Gomez Maqueo Chew Y., Pollacco D., Stassun K., Collier Cameron A., 2012, in American Astronomical Society Meeting Abstracts #219. p. 345.15
Henden A., Munari U., 2014, Contrib. Astron. Obs. Skalnate Pleso, 43, 518
Holman M. J. et al., 2006, ApJ, 652, 1715
Huang C. X. et al., 2018, ApJ, 868, L39
Jenkins J. M. et al., 2016, Proc. SPIE 99133, Software and Cyberinfrastructure for Astronomy IV, 99133E
Kaufer A., Stahl O., Tubbesing S., Nørregaard P., Avila G., Francois P., Pasquini L., Pizzella A., 1999, The Messenger, 95, 8
Kreidberg L., 2015, PASP, 127, 1161
Lendl M. et al., 2012, A&A, 544, A72
Lendl M., Cubillos P. E., Hagelberg J., Müller A., Juvan I., Fossati L., 2017, A&A, 606, A18
Mann A. W., Feiden G. A., Gaidos E., Boyajian T., von Braun K., 2015, ApJ, 804, 64
Nielsen L. D. et al., 2019, A&A, 623, A100
Ofir A., Gandolfi D., Buchhave L., Lacy C. H. S., Hatzes A. P., Fridlund M., 2012, MNRAS, 423, L1
Osborn H. P. et al., 2016, MNRAS, 457, 2273
Pepe F. et al., 2002, The Messenger, 110, 9
Queloz D. et al., 2001, The Messenger, 105, 1
Ricker G. R. et al., 2014, in Oschmann Jr. J. M., Clampin M., Fazio G. G., MacEwen H. A., eds, Proc. SPIE Conf. Ser. Vol. 9143, Space Telescopes and Instrumentation 2014: Optical, Infrared, and Millimeter Wave. SPIE, Bellingham, p. 914320
Schlegel D. J., Finkbeiner D. P., Davis M., 1998, ApJ, 500, 525
Skrutskie M. F. et al., 2006, AJ, 131, 1163
Smith J. C. et al., 2012, PASP, 124, 1000
Southworth J., 2009, MNRAS, 394, 272
Stassun K. G., Torres G., 2016, ApJ, 831, L6
Stassun K. G., Torres G., 2018, ApJ, 862, 61
Stassun K. G., Collins K. A., Gaudi B. S., 2017, AJ, 153, 136
Stassun K. G., Corsaro E., Pepper J. A., Gaudi B. S., 2018, AJ, 155, 22
Stumpe M. C., Smith J. C., Catanzarite J. H., Van Cleve J. E., Jenkins J. M., Twicken J. D., Girouard F. R., 2014, PASP, 126, 100
Tamuz O., Mazeh T., Zucker S., 2005, MNRAS, 356, 1466
Tokovinin A., 2018, PASP, 130, 035002
Torres G., Andersen J., Giménez A., 2010, A&AR, 18, 67
Villanueva S., Jr., Dragomir D., Gaudi B. S., 2019, AJ, 157, 84
Wang S. et al., 2019, AJ, 157, 51
Wheatley P. J. et al., 2018, MNRAS, 475, 4476
Winn J. N. et al., 2008, ApJ, 683, 1076
Wittenmyer R. A., Horner J., Carter B. D., Kane S. R., Plavchan P., Ciardi D., MINERVA–Australis consortium t., 2018, preprint (arXiv:1806.09282)
Wright E. L. et al., 2010, AJ, 140, 1868
Zacharias N., Finch C. T., Girard T. M., Henden A., Bartlett J. L., Monet D. G., Zacharias M. I., 2013, AJ, 145, 44
Ziegler C., Tokovinin A., Briceno C., Mang J., Law N., Mann A. W., 2019, AJ, 159, 19

SUPPORTING INFORMATION

Supplementary data are available at *MNRAS* online.

Table 2. EulerCam photometry.
Table 3. NGTS photometry, binned into 2-min intervals.

Please note: Oxford University Press is not responsible for the content or functionality of any supporting materials supplied by the authors. Any queries (other than missing material) should be directed to the corresponding author for the article.

[1]*Observatoire de Genève, Université de Genève, 51 Ch. des Maillettes, CH-1290 Sauverny, Switzerland*
[2]*Space Research Institute, Austrian Academy of Sciences, Schmiedlstr 6, A-8042 Graz, Austria*
[3]*Department of Physics, University of Warwick, Gibbet Hill Road, CV4 7AL Coventry, UK*
[4]*Centre for Exoplanets and Habitability, University of Warwick, Gibbet Hill Road, CV4 7AL Coventry, UK*
[5]*Deparment of Physics & Astronomy, Vanderbilt University, 6301 Stevenson Center Ln., Nashville, TN 37235, USA*
[6]*Department of Physics, Fisk University, 1000 18th Ave. N., Nashville, TN 37208, USA*
[7]*Department of Physics and Astronomy, University of Leicester, University Road, LE1 7RH Leicester, UK*
[8]*Institute of Planetary Research, German Aerospace Center, Rutherford-strasse 2, D-12489 Berlin, Germany*
[9]*Astrophysics Group, Cavendish Laboratory, J.J. Thomson Avenue, CB3 0HE Cambridge, UK*
[10]*Department of Physics, and Kavli Institute for Astrophysics and Space Research, Massachusetts Institute of Technology, Cambridge, MA 02139, USA*
[11]*Departamento de Astronomia, Universidad de Chile, Casilla 36-D, Santiago, Chile*
[12]*Centro de Astrofísica y Tecnologías Afines (CATA), Casilla 36-D, Santiago, Chile*
[13]*Instituto de Astronomía, Universidad Católica del Norte, Angamos 0610, 1270709, Antofagasta, Chile*
[14]*Center for Astrophysics, Harvard & Smithsonian, 60 Garden St, Cambridge, MA 02138, USA*
[15]*Department of Earth, Atmospheric and Planetary Sciences, Massachusetts Institute of Technology, Cambridge, MA 02139, USA*
[16]*Department of Aeronautics and Astronautics, MIT, 77 Massachusetts Avenue, Cambridge, MA 02139, USA*
[17]*Department of Astrophysical Sciences, Princeton University, Princeton, NJ 08544, USA*
[18]*NASA Ames Research Center, Moffett Field, CA 94035, USA*
[19]*University of Southern Queensland, Centre for Astrophysics, West Street, Toowoomba, QLD 4350 Australia*
[20]*Cerro Tololo Inter-American Observatory, Casilla 603, La Serena, Chile*

[21]*Center of Astro-Engineering UC, Pontificia Universidad Católica de Chile, Av. Vicuña Mackenna 4860, 7820436 Macul, Santiago, Chile*
[22]*Millennium Institute for Astrophysics, Santiago,Chile*
[23]*SETI Institute, 189 Bernardo Ave., Suite 200, Mountain View, CA 94043, USA*
[24]*Noqsi Aerospace Ltd., 15 Blanchard Avenue, Billerica, MA, 01821, USA*
[25]*Space Telescope Science Institute, 3700 San Martin Drive, Baltimore, MD 21218, USA*
[26]*Max-Planck-Institut für Astronomie, Königstuhl 17, D-69117 Heidelberg, Germany*
[27]*Facultad de Ingeniería y Ciencias, Universidad Adolfo Ibáñez, Av. Diagonal las Torres 2640, Peñalolén, Santiago, Chile*
[28]*Department of Physics and Astronomy, The University of North Carolina at Chapel Hill, Chapel Hill, NC 27599-3255, USA*
[29]*NASA Goddard Space Flight Center, 8800 Greenbelt Road, MD, USA*
[30]*Dunlap Institute for Astronomy and Astrophysics, University of Toronto, 50 St George Street, Toronto, ON M5S 3H4, Canada*

This paper has been typeset from a TEX/LATEX file prepared by the author.